Supporting Information

Reactive Spinning to Achieve Nanocomposite Gel Fibers: from Monomer to Fiber Dynamically with Enhanced Anisotropy

Peiling Wei,[a] Kai Hou, [a] Tao Chen, [a] Guoyin Chen, [a] Innocent Tendo Mugaanire[a] and Meifang Zhu*[a]

[a] *State Key Laboratory for Modification of Chemical Fibers and Polymer Materials, College of Materials Science and Engineering, Donghua University, Shanghai 201620, China.*

Experiments

1.1 Characterization of reaction kinetics of gelation process.

Rheological Measurement. In order to monitor the reaction kinetics in gelation process of precursor solution for $GH-Fibers^{12-0.2(0.8)}_{x}$, the rheological measurements were performed with a stress-controlled rheometer Physica MCR 302 (Anton Paar, Germany) in parallel plate mode (diameter is 25 mm). The test was carried out by dynamic time sweep measurements in 15 minutes at 22 ℃, with strain set as 1% and the angular frequency set as 6.28 rad/s. The measurement was performed with precursor solution transferred onto the parallel plate and quickly mixed with TEMED. And the gap between parallel plates was 0.5 mm.

NMR measurement. ^{1}HNMR measurement was acquired with a Bruker Avance-600 MHz spectrometer. To monitor the time dependent gelation process of precursor solution for $GH-Fibers^{12-0.2(0.8)}_{x}$, the time dependent ^{1}HNMR spectra was carried out and obtained every 2 min in reaction time range from 5 min to 15 min with temperature at 25 ℃. In this measurement, precursor solution was prepared in D_2O to reduce interference peaks from solvent.

1.2 Characterization of the structure and properties of Fibers

Transmission electron microscope (TEM). The morphology of clay (Laponite XLS) was imaged by TEM (JEM-2100F), with clay samples collected on 400 mesh carbon-coated copper grid.

Attenuated Total Reflectance Fourier transform infrared spectroscopy (ATR-FTIR). ATR-FTIR spectra were carried out by Nicolet 6700 infrared spectrometer (Thermo Fisher, 4100 to 600 cm^{-1}). Before measurement, fiber samples were dried at 80 ℃ for 24 h to remove H_2O.

Morphologies and diameters. Field emission scanning electron microscope (FE-SEM, JEOL SU8010) was used to observe the surface and cross-sectional morphologies of fibers. Before SEM observation, the samples should be frozen-dried and gold-sprayed. Optical microscope (Nikon Eclipse Ni) was used to observe the knotted $GH-Fibers^{12-0.2(0.8)}_{109}$ in crossed polarized mode with sample angle of 45 °. The diameters of $GH-Fibers^{12-0.2(0.8)}_{x}$ from varied spinning parameters were recorded via optical microscope (VHM2600, VIHENT) equipped with a CCD camera.

Wide-Angle X-ray Diffraction (WAXD). 2D WAXD images of samples were obtained at the BL15U1 beamlines at the Shanghai Synchrotron Radiation Facility (SSRF). SSRF has an energy ring of 3.5 GeV and a beam current of 220 mA. For 2D WAXD, the wavelength (λ) of the X-rays and the sample spot size were 0.07746 nm and 10 × 10 μm^2, respectively. The corresponding 1D WAXD spectra were calculated from the integral of 2D WAXD via Fit2D software

from the European Synchronization Radiation Facility.

Small-Angle X-ray Scattering (SAXS). SAXS patterns for fibers were obtained by Small Angle X-ray scatter (Anton Paar SAXSess mc2, voltage was 40 kV, current was 50 mA, data acquisition time was 20 min, point source of light). The equipment provided only half of the patterns, and a symmetric process was applied in the manuscript for better comparison.

Mechanical properties. Mechanical properties of $GH-Fibers^{12-0.2(0.8)}_{x}$ produced with different winding speed (0 m/h, 25 m/h, 54 m/h, 77 m/h, 109 m/h, 128 m/h) were tested by a monofilament strength meter (XQ-1A, Shanghai Lipu Applied Science Institute). The tensile gauge length was 10 mm with tensile speed at 20 mm/min. Mechanical properties of $GH-Fibers^{c-0.2(0.8)}_{109}$ with different clay content (8 wt.%, 10 wt.%, 12 wt.%, 14 wt.%) were performed on an universal test machine Instron 5969 with gauge length at 10 mm and tensile speed at 50 mm/min. Mechanical properties of $GH-Fibers^{12-0.2(0.8)}_{109}$ and $H-Fibers^{12-0.2(0.8)}_{109}$ were tested by a monofilament strength meter (XQ-1A, Shanghai Lipu Applied Science Institute) after stored at 22 ℃ (~35% humidity) for 2 h, 1 day and 30 days, respectively. The tensile gauge length was 10 mm and tensile speed was 50 mm/min. The mechanical properties of hydrogels with pure monomer ($GH-Gel^{12-1(0)}$and $GH-Gel^{12-0(1)}$) and comonomer ($GH-Gel^{12-0.2(0.8)}$) were also measured by a monofilament strength meter (XQ-1A, Shanghai Lipu Applied Science Institute), with gauge of 5 mm and tensile speed of 50 mm/min. These stable hydrogels were prepared with precursor solutions (with the addition of TEMED) casted in plastic mold (inner diameter at 5 mm) for 24 h at 22 ℃, and their nomenclatures and components were also shown in **Table S1**. The Young's modulus (E) is defined as the slope of the strain stress curves in 0-10% strain (ε). The fracture energy (U_f) at break is calculated by integrating the area at fracture under the stress-strain curves as follows:

$$U_f = \int_0^{\varepsilon} \sigma d\varepsilon$$

Tensile strength at break (σ), Young's modulus (E) and fracture energy (U_f) of fibers were recorded from the average results of at least 3 experiments.

Stability of GH-Fibers and H-Fibers. Solvent loss of $GH-Fibers^{12-0.2(0.8)}_{109}$ and $H-Fibers^{12-0.2(0.8)}_{109}$ was recorded by weightlessness method at temperature at 22 ℃ and humidity at ~35% in 30 days. The results of weight retention for such fibers were calculated from the average results of 3 samples, via the following equation:

$$weight\ retention = \frac{w_t}{w_0}$$

Where w_t stands for the weight of fibers at real time, and w_0 stands for the initial weight of corresponding fibers. The liquid loss of fibers was calculated from the equation:

$$\text{Liquid loss} = \left(1 - \frac{w_t}{w_0}\right) \times 100\%$$

Swelling behaviors of GH-Fibers. As-prepared $GH-Fibers^{12-0.2(0.8)}_{109}$ was cut into sections of 30 mm in length.

Then, $GH-Fibers^{12-0.2(0.8)}_{109}$ was immersed in a large excess of water at 25 °C, and the weight of such swollen fibers was measured in real for 480 s. The time dependence for weight ratio of swollen GH-Fibers was represented by:

$$Swollen\ weight\ ratio = \frac{W_{st}}{W_0} \times 100\%$$

Where W_{st} stands for the weight of swollen GH-Fibers at real time, and W_0 stands for the initial weight of GH-Fibers.

Dynamic mechanical analysis (DMA). Elastic (E') and viscous modulus (E'') of fibers were measured via a dynamic mechanical analysis (DMA 1, METTLER TOLEDO) in tension mode. The $GH-Fibers^{12-0.2(0.8)}_{109}$ length was set at 10 mm, with diameter of 250 μm. In measurement, the frequency was set at 1 Hz, load set at 0.05N, and auto-strain was set at 150%. The temperature range was from -40 to 10 ℃ with heating rate at 1 ℃·min^{-1}.

Differential scanning calorimetry (DSC) analysis. The anti-freezing property of fibers were conducted using differential scanning calorimetry analysis (DSC 1, METTLER TOLEDO). Fiber samples including $GH-Fibers^{12-0.2(0.8)}_{109}$, $H-Fibers^{12-0.2(0.8)}_{109}$, and GH-Fibers with 10 wt.% and 30 wt.% glycerol: $GH-Fibers^{12-0.2(0.8)}_{109}-10\%$ and $GH-Fibers^{12-0.2(0.8)}_{109}-30\%$. And the anti-freezing behaviors of corresponding clay dispersions for $GH-Fibers^{12-0.2(0.8)}_{109}$, $H-Fibers^{12-0.2(0.8)}_{109}$, in H_2O and glycerol/H_2O (1/4, w/w), respectively, were also performed to investigate the influence of solvent on freezing point of fibers. The temperature was measured from -70 ℃ to 10 ℃ with a heating rate of 5 °C·min^{-1}. The samples were kept under inert environment using continuous nitrogen gas purging at flow rate of 50 ml·min^{-1}.

Figures and results

Table S1 Compositions of all fibers and hydrogels

Samples	H_2O (g)	Glycerol (g)	Clay (g)	OEGMA (g)	DMAA (g)	KPS (g)	TEMED (μL)
$GH-Fibers^{12-0(1)}_{x}$	4.0	1.0	0.6	0.00	1.00	0.015	35
$GH-Fibers^{12-0.1(0.9)}_{x}$	4.0	1.0	0.6	0.36	0.64	0.015	35
$GH-Fibers^{12-0.2(0.8)}_{x}$	4.0	1.0	0.6	0.56	0.44	0.015	35
$GH-Fibers^{12-0.4(0.6)}_{x}$	4.0	1.0	0.6	0.77	0.23	0.015	35
$GH-Fibers^{12-0.6(0.4)}_{x}$	4.0	1.0	0.6	0.88	0.12	0.015	35
$GH-Fibers^{12-0.8(0.2)}_{x}$	4.0	1.0	0.6	0.95	0.05	0.015	35
$GH-Fibers^{12-0.9(0.1)}_{x}$	4.0	1.0	0.6	0.98	0.02	0.015	35
$GH-Fibers^{12-1(0)}_{x}$	4.0	1.0	0.6	1.00	0.00	0.015	35
$GH-Fibers^{8-0.2(0.8)}_{109}$	4.0	1.0	0.4	0.56	0.44	0.015	35
$GH-Fibers^{10-0.2(0.8)}_{109}$	4.0	1.0	0.5	0.56	0.44	0.015	35

$GH-Fibers^{14-0.2(0.8)}_{109}$	4.0	1.0	0.7	0.56	0.44	0.015	35
$H-Fibers^{12-0.2(0.8)}_{109}$	5.0	0.0	0.6	0.56	0.44	0.015	35
$GH-Fibers^{12-0.2(0.8)}_{109}$ -10%	4.5	0.5	0.6	0.56	0.44	0.015	35
$GH-Fibers^{12-0.2(0.8)}_{109}$ -30%	3.5	1.5	0.6	0.56	0.44	0.015	35
$GH-Gel^{12-1(0)}$	4.0	1.0	0.6	1.00	0.00	0.015	35
$GH-Gel^{12-0.2(0.8)}$	4.0	1.0	0.6	0.56	0.44	0.015	35
$GH-Gel^{12-0(1)}$	4.0	1.0	0.6	0.00	1.00	0.015	35

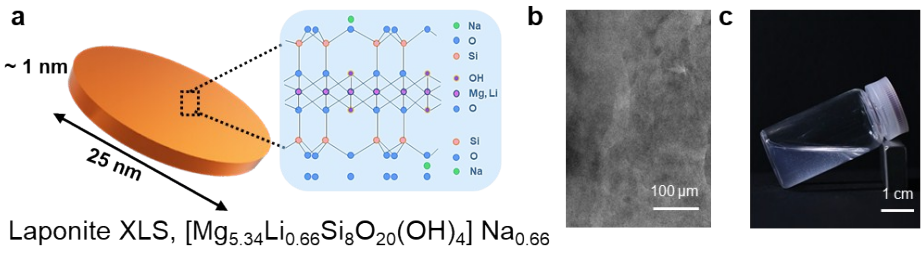

Figure S1 (a) Illustration of the ideal structure and (b) TEM image of Laponite XLS, (c) the digital image of precursor solution for $GH-Fibers^{12-0.2(0.8)}_{x}$.

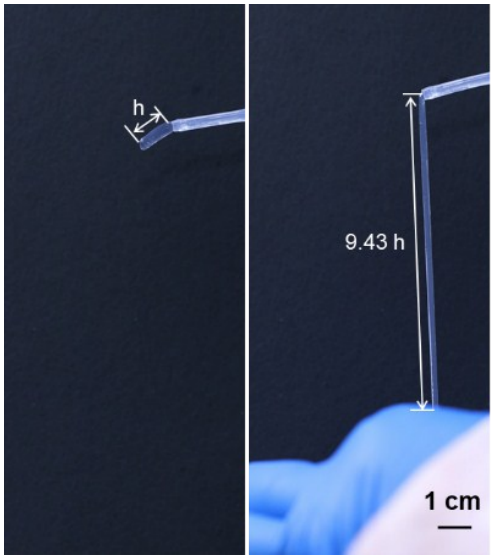

Figure S2 Images of squeezed pre-gel for $GH-Fibers^{12-0.2(0.8)}_{x}$ after 13 minutes keeping in PTFE pipe from precursor solution. (a) pre-gel squeezed out of pipe, (b) the elongation of the squeezed pre-gel in stretching. Here, the pre-gel showed weak flowability and low stretching ratio (fractured at around 943%), due to the restrictions of relative stable three-dimensional clay-polymer networks.

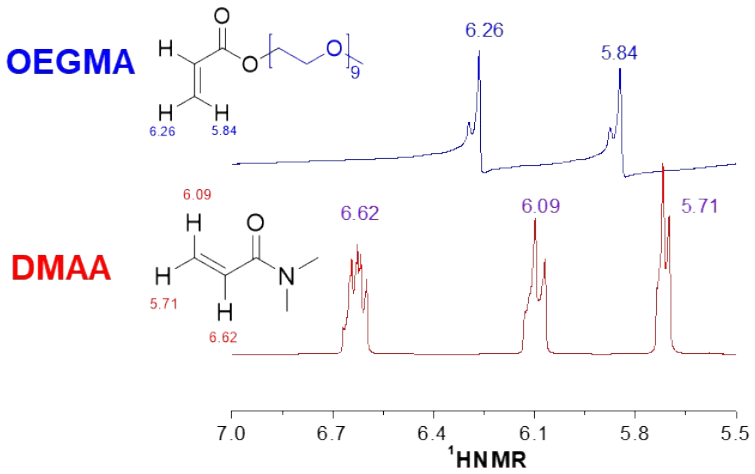

Figure S3 ^{1}HNMR spectra of OEGMA and DMAA monomers in D_2O.

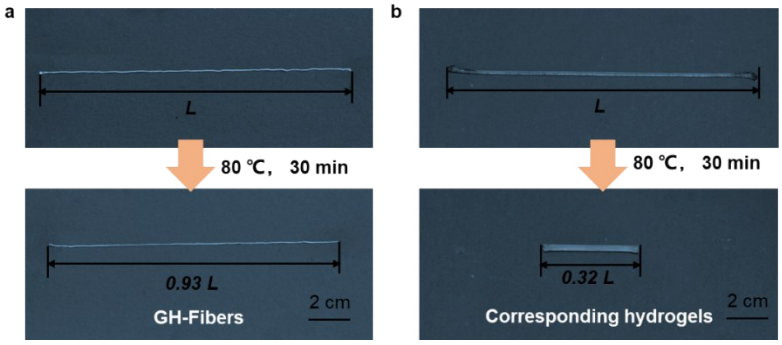

Figure S4 (a) Low resilience ability of $GH-Fibers^{12-0.2(0.8)}_{109}$, whose initial length was L and retained 0.93 L after heated for 30 min at 80 ℃. (b) Large resilience of corresponding stable hydrogel $GH-Fibers^{12-0.2(0.8)}_{0}$, whose initial length was 0.27 L, and recovered to 0.32 L after heated at 80 ℃ in 30 minutes when stretched to L.

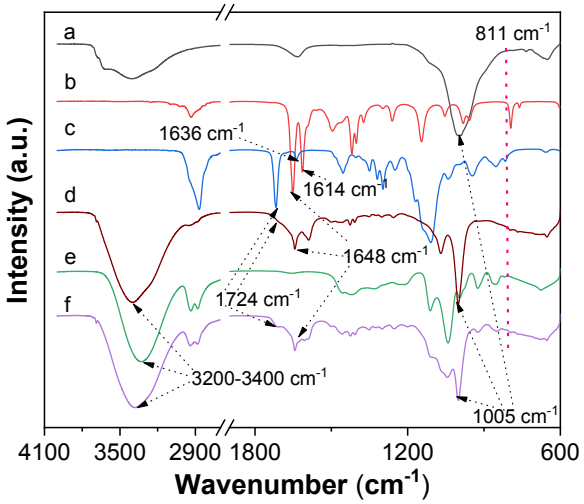

Figure S5 FTIR spectra of (a) clay, (b) DMAA, (c) OEGMA, (d) $H-Fibers^{12-0.2(0.8)}_{109}$, (e) glycerol, and (f) $GH-Fibers^{12-0.2(0.8)}_{109}$.

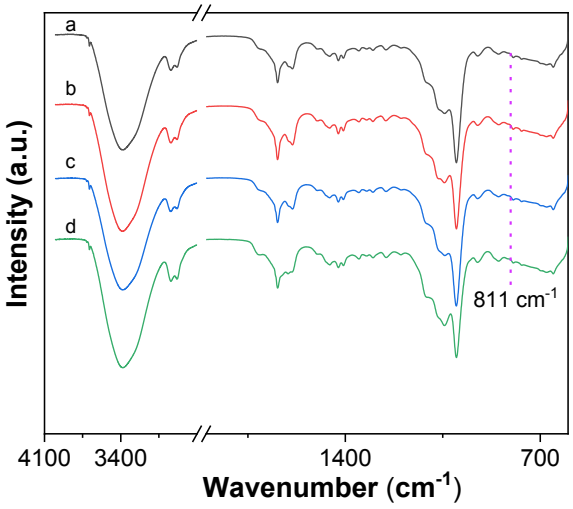

Figure S6 FTIR spectra of $GH-Fibers_{109}^{12-0.2(0.8)}$ from different squeezing time. (a) 7 min, (b) 8 min, (c) 9 min, (d) 10 min. Similar spectra were shown for such GH-Fibers irrespectively of squeezed time.

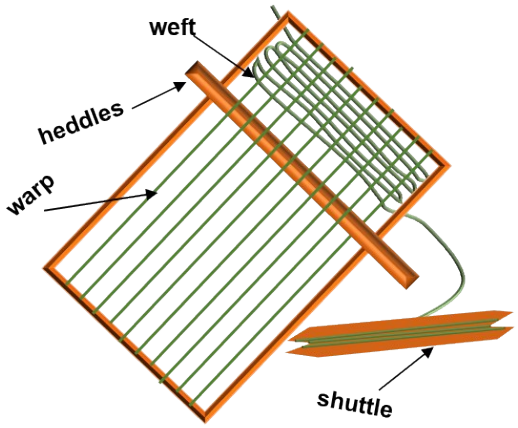

Figure S7 Illustration of the manual knitting machine consisting of shuttle, heddles, weft and warp.

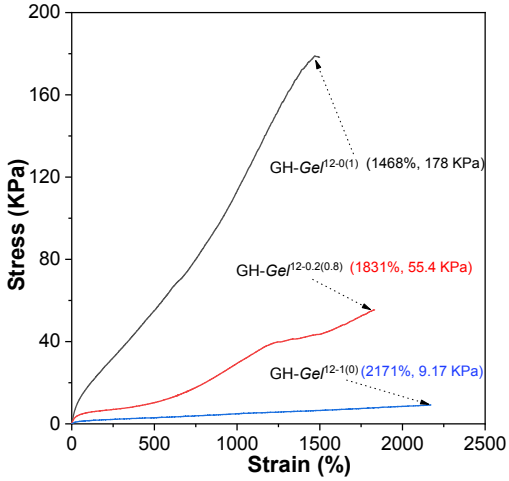

Figure S8 Tensile property of hydrogels formed in plastic mold with diverse monomer ratio. With pure DMAA, $GH-Gel^{12-0(1)}$ show high tensile stress with relative short extensions, while $GH-Gel^{12-1(0)}$ with pure OEGMA

displayed long extensions and relatively low tensile stress.

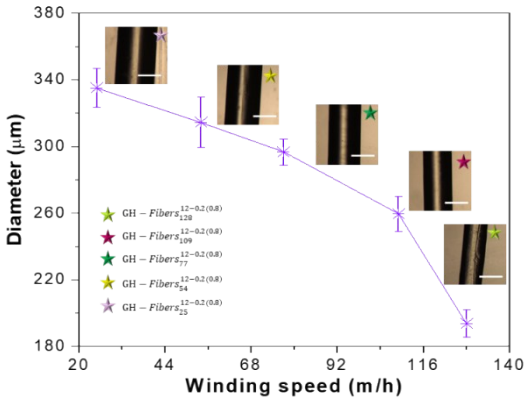

Figure S9 Adjustable diameters of $GH-Fibers_{x}^{12-0.2(0.8)}$ via different winding speeds within a range of 25 to 128 m/h. The insert pictures showed morphologies of the $GH-Fibers_{x}^{12-0.2(0.8)}$ fabricated via corresponding winding speed. (the scale bar is 200 μm).

Table S2 Spinnability of GH-Fibers with diverse molar ratio of OEGMA in monomer and varied winding speed.

Samples	Winding speed (m/h)				
	25	**54**	**77**	**109**	**128**
$GH-Fibers_{x}^{12-0(1)}$	-	-	-	-	-
$GH-Fibers_{x}^{12-0.1(0.9)}$	+	+	+	+	+
$GH-Fibers_{x}^{12-0.2(0.8)}$	+	+	+	+	+
$GH-Fibers_{x}^{12-0.4(0.6)}$	+	+	+	+	-
$GH-Fibers_{x}^{12-0.6(0.4)}$	+	+	+	+	-
$GH-Fibers_{x}^{12-0.8(0.2)}$	+	+	+	-	-
$GH-Fibers_{x}^{12-0.9(0.1)}$	-	-	-	-	-
$GH-Fibers_{x}^{12-1(0)}$	-	-	-	-	-

In this table, "+" represents the spinnability, and "-" represents the non-spinnability of $GH-Fibers_{x}^{12-y(1-y)}$, respectively.

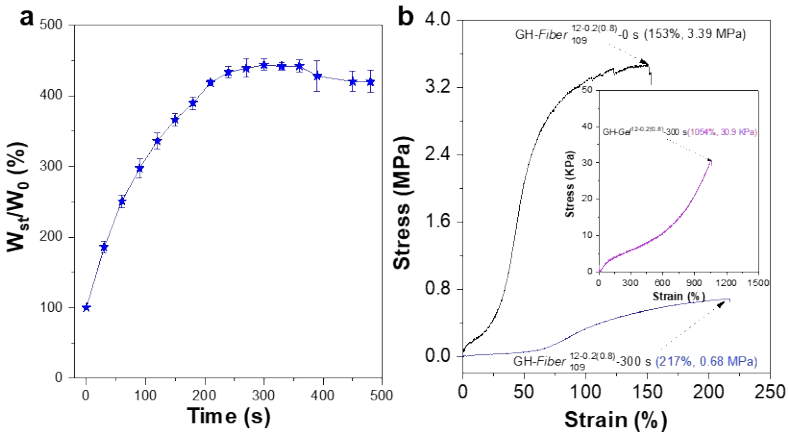

Figure S10 Mechanical behaviors of GH-Fibers in water. (a) Swelling behaviors of $GH-Fiber^{12-0.2(0.8)}_{109}$ in water, displayed rapid swelling behaviors in water, which reached equilibrium swollen (~420%) within about 240 s. (b) Stress-strain curves of $GH-Fiber^{12-0.2(0.8)}_{109}$ with different swelling time: 0 s, and 300 s, inserted figures: $GH-Gel^{12-0.2(0.8)}$ swelling in water for 300 s.

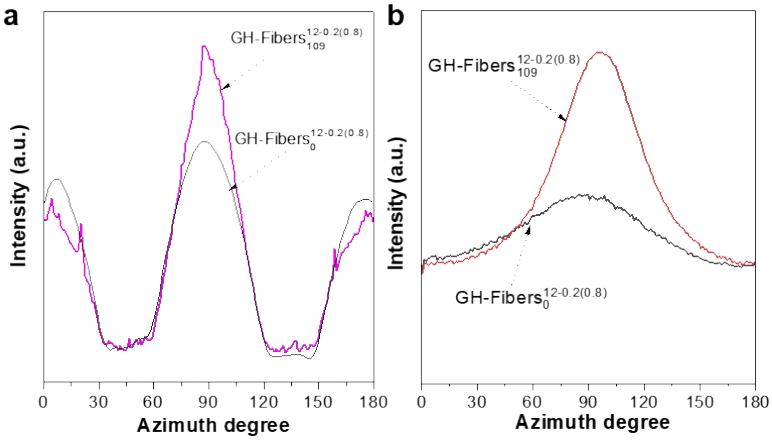

Figure S11 (a) 1D WXRD and (b) SAXS spectra of $GH-Fibers^{12-0.2(0.8)}_{0}$ and $GH-Fibers^{12-0.2(0.8)}_{109}$ in different azimuth degree, which were calculated from 2D WXRD and SAXS patterns in **Figure 3d** and **Figure 3e** of the manuscript.

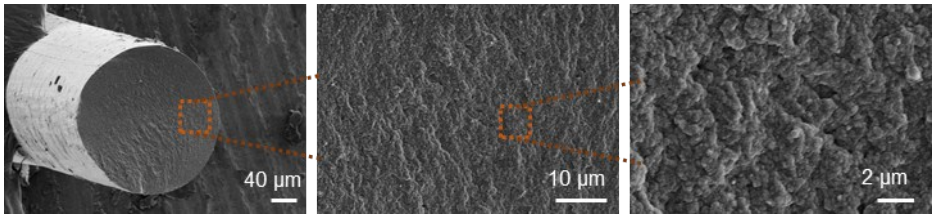

Figure S12 SEM images of $GH-Fibers^{12-0.2(0.8)}_{109}$ with compact stacked structures in different magnifications. (a) 350 ×, (b)2000 ×, (c) 8000 ×.

Table S3 Mechanical properties of GH-Fibers from different spinning parameters

Samples	Elongation (%)	Tensile stress (MPa)	Young's modulus (MPa)	Fracture energy [KJ·m^{-2}]
$GH-Fibers^{12-0.2(0.8)}_{0}$	2086 ± 19.00	0.078 ± 0.005	0.084 ± 0.017	3.80^{0} ± 0.573
$GH-Fibers^{12-0.2(0.8)}_{25}$	528.2 ± 32.72	1.140 ± 0.122	0.965 ± 0.103	45.90 ± 6.058
$GH-Fibers^{12-0.2(0.8)}_{54}$	235.0 ± 16.31	1.288 ± 0.048	1.527 ± 0.213	28.75 ± 3.510
$GH-Fibers^{12-0.2(0.8)}_{77}$	208.6 ± 20.91	1.800 ± 0.058	2.660 ± 0.320	27.69 ± 3.261
$GH-Fibers^{12-0.2(0.8)}_{109}$	149.4 ± 6.520	3.357 ± 0.089	4.072 ± 0.183	38.79 ± 5.742
$GH-Fibers^{12-0.2(0.8)}_{128}$	147.7 ± 23.78	5.250 ± 0.082	5.300 ± 0.274	50.33 ± 6.464

All results are calculated from at least 3 experiments.

Table S4 Mechanical properties of GH-Fibers with different clay content.

Sample	Elongation (%)	Tensile stress (MPa)	Elastic modulus (MPa)	Fracture energy [kJ·m^{-2}]
$GH-Fibers^{8-0.2(0.8)}_{109}$	270.1 ± 26.91	1.16 ± 0.05	1.074 ± 0.400	29.95 ± 4.005
$GH-Fibers^{10-0.2(0.8)}_{109}$	201.4 ± 9.847	2.93 ± 0.13	5.632 ± 0.653	44.05 ± 2.080
$GH-Fibers^{12-0.2(0.8)}_{109}$	150.7 ± 16.36	3.71 ± 0.11	8.582 ± 0.751	43.09 ± 3.441
$GH-Fibers^{14-0.2(0.8)}_{109}$	163.6 ± 8.894	7.20 ± 0.06	16.14 ± 1.168	79.90 ± 4.686

All results are calculated from at least 3 experiments.

Table S5 Comparison of Young's modulus and tensile stress of GH-Fibers with other gel systems and natural soft tissues.

Gel systems	Tensile stress (KPa)	Young's Modulus (KPa)	References
PDMAA/clay	25-300	1-30	1
PMDMAEA-Q/PNaSS	800-5100	280-7900	2
Upy-PEG	300-1500	310-2070	3

Alginate-AAm	30-200	10-100	4
GO/PAA	272-777	32-51	5
Agar-PAAm	423-745	13-313	6
Clay/PAA/Fe^{3+}	800-3500	100-1000	7
PNAGA	167-1143	48-153	8
Tetra-PEG/RGO	100-600	10-110	9
Skeletal muscle	100-350	10000-60000	10
Cartilage	800-25000	5000-25000	11
GH-Fibers	1160-7200	1074-16140	Our work

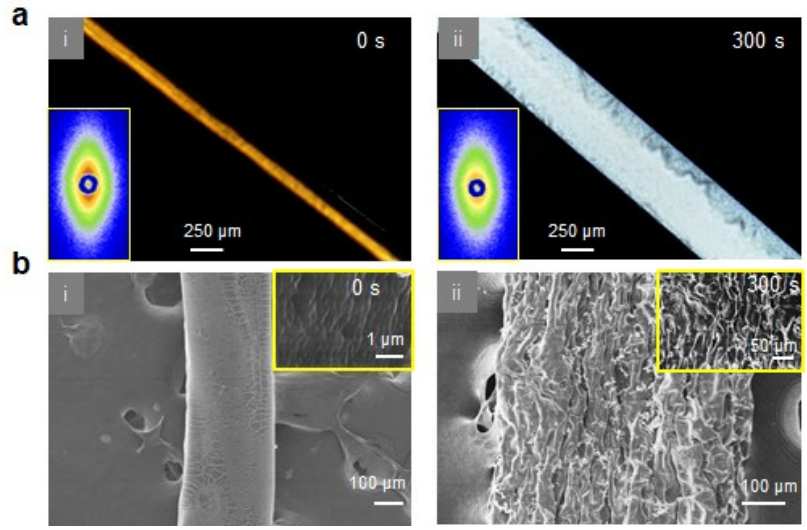

Figure S13 Anisotropy of GH-Fibers when immersed in water. (a) Polarizing microscope images and corresponding SAXS patterns (inserted figures), and (b) SEM images of $GH-Fiber^{12-0.2(0.8)}_{109}$ after swelling in water for 0 s (i) and 300 s (ii), respectively.

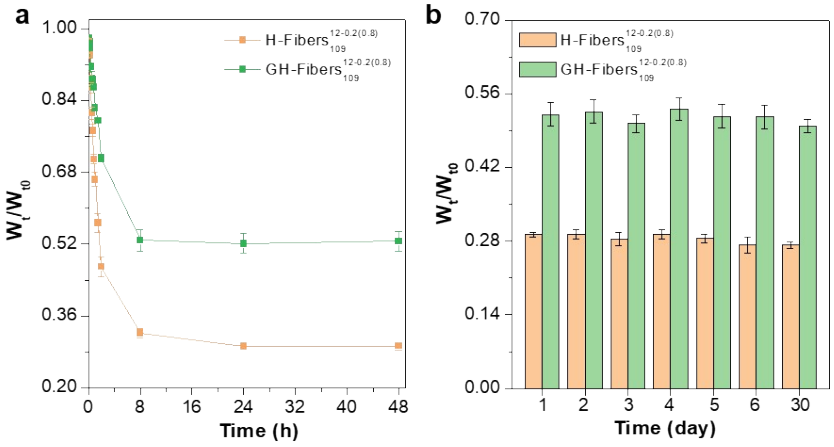

Figure S14 Weight loss of GH-Fibers and H-Fibers. (a) Fast liquid evaporation in $GH-Fibers^{12-0.2(0.8)}_{109}$ and

$H-Fibers^{12-0.2(0.8)}_{109}$ in 24 h to reach a balance. (b) The stable weight retention for $GH-Fibers^{12-0.2(0.8)}_{109}$ was at ~52% and for $H-Fibers^{12-0.2(0.8)}_{109}$ at ~28% after 30 days.

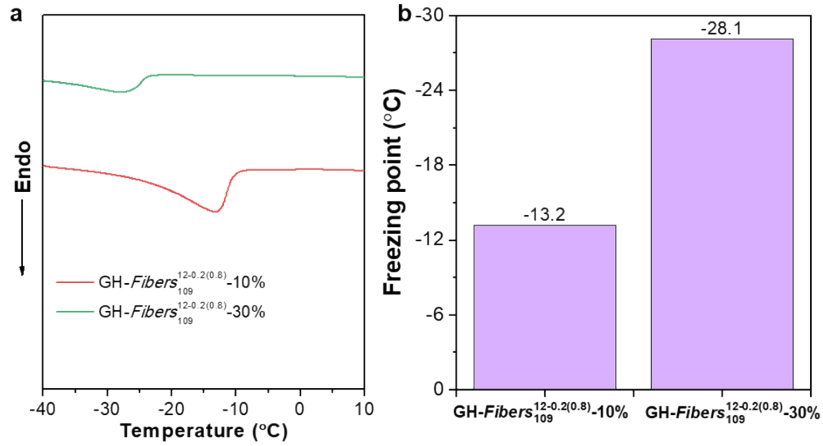

Figure S15 Adjustable anti-freezing property of GH-Fibers by glycerol ratio. (a) DSC curves, and (b) corresponding freezing points of $GH-Fibers^{12-0.2(0.8)}_{109}-10\%$ and $GH-Fibers^{12-0.2(0.8)}_{109}-30\%$ in temperature range of -40 to 10 ℃. The freezing point of GH-Fibers reduced from -13.2 ℃ to -28.1 ℃ with the increase of glycerol ratio from 10 wt.% to 30 wt.%.

References

1. K. Haraguchi, R. Farnworth, A. Ohbayashi, T. Takehisa, *Macromolecules*, 2003, **36**, 5732-5741.
2. F. Luo, T. L. Sun, T. Nakajima, T. Kurokawa, Y. Zhao, K. Sato, A. B. Ihsan, X. Li, H. Guo, J. P. Gong, *Advanced Materials*, 2015, **27**, 2722-2727.
3. M. Guo, L. M. Pitet,H. M. Wyss, M. Vos, P. Y. Dankers, E. W. Meijer, *Journal of the American Chemical Society*, 2014, **136**, 6969-6977.
4. J. Y. Sun, X. Zhao, W. R. Illeperuma, O. Chaudhuri, K. H. Oh, D. J. Mooney, J. J. Vlassak, Z. Suo, *Nature*, 2012, **489**, 133-136.
5. M. Zhong, Y.-T. Liu, X.-M. Xie, *Journal of Materials Chemistry B*, 2015, **3**, 4001-4008.
6. Q. Chen, D. Wei, H. Chen, L. Zhu, C. Jiao, G. Liu, L. Huang, J. Yang, L. Wang, J. Zheng, *Macromolecules*, 2015, **48**, 8003-8010.
7. Y. Hu, Z. Du, X. Deng, T. Wang, Z. Yang, W. Zhou, C. Wang, *Macromolecules*, 2016, **49**, 5660-5668.
8. X. Dai, Y. Zhang, L. Gao, T. Bai, W. Wang, Y. Cui, W. Liu, *Advanced Materials*, 2015, **27**, 3566-3571.
9. L. Wang, K. Lei, Z. Li, X. Wang, H. Xiao, Z. Zheng, *Macromolecular Materials and Engineering*, 2018, **303**, 1800325.
10. T. Mirfakhrai, J. D. W. Madden, R. H. Baughman, *Materials Today*, 2007, **10**, 30-38.
11. C. J. Little, N. K. Bawolin, X. Chen, *Tissue Engineering Part B: Reviews*, 2011, **17**, 213-227.